Appl. Phys. A (2017) 123:705
DOI 10.1007/s00339-017-1327-1

Applied Physics A
Materials Science & Processing

# Microindentation on the porous copper surface modulations

**Dursun Ekmekci[1] · Fikret Yılmaz[2] · Uğur Kölemen[2,3] · Ömer Necati Cora[4]**

Received: 21 June 2017 / Accepted: 13 October 2017 / Published online: 20 October 2017
© Springer-Verlag GmbH Germany 2017

**Abstract** This study aimed to investigate the mechanical properties of a surface modulation which was realized through compaction, and then sintering of copper powders. To this goal, Berkovich type of indenter and depth-sensing indentation technique were used in microindentation to measure the hardness and modulus of elasticity values at different features of compact. Indentations were performed with a peak force of 50 mN. Hardness values were obtained in 0.88–1.12 GPa range while the modulus of elasticity was recorded in the 70–111 GPa interval. Even though both modulus of elasticity and hardness values were noted to be different for copper powders and substrate, one-way ANOVA analyses showed that the differences in both modulus of elasticity and hardness values are insignificant. FE modeling of microindentation was also performed and validated. It was shown that the force–displacement values obtained from FE analyses are quite well in agreement with the experimental data.

✉ Ömer Necati Cora
oncora@ktu.edu.tr

[1] Department of Mechanical Engineering, Gümüşhane University, 29100 Gümüşhane, Turkey

[2] Department of Physics, Faculty of Arts and Science, Gaziosmanpaşa University, 60240 Tokat, Turkey

[3] Faculty of Arts and Science, Giresun University, 28200 Giresun, Turkey

[4] Department of Mechanical Engineering, Karadeniz Technical University, 61080 Trabzon, Turkey

## 1 Introduction

The miniaturization trend in electronics industry forces manufacturers to increase heat dissipation rates per unit area to avoid system temperature rising significantly which may lead to malfunctioning and breakdown of entire device [1]. Pure copper is known to have the highest electrical conductivity among the commercially available metals. In addition, thanks to its high ductility, malleability, thermal conductivity and resistance to corrosion it is the prominent choice of material in several industries including electronics, power, and telecommunication. The most common applications are cables, printed circuit board conductors, and wires. Copper alloys are also preferred in heat exchangers and thermal management systems in electronics. It was noted that thermal conductivity of copper is about twice of that for aluminum (403 vs. 237 W/m °C) [2]. Therefore, much more heat can be dissipated more quickly using copper. It is, therefore, the preferred material in super computer chips so that the processer operates with higher efficiently, and less potential for damage to other critical components [3].

Porous copper and copper powders are frequently preferred in heat exchangers as those have increased surface area so the heat transfer rate and copper's high thermal conductivity. It was shown by researches that the microscale porous and modulated surfaces enhance heat transfer efficiencies by 300% compared to plain surfaces [4, 5]. Moreover, thin films such as pure copper usually are reported to have distinct mechanical and tribological properties compared to bulk materials. As a result, measurement and understanding of these interactions in micro/nanoscale is critical. Nevertheless, it is impossible to evaluate the mechanical properties of such films, and structures having sub-micron-scale features by conventional testing methods.

Instrumented indentation is a useful tool to acquire mechanical properties such as modulus of elasticity and hardness of ultra-thin films in small volumes [6–9]. It was reported by Xue et al. that yield strength increases as the hardness value increases, and the elongation decreases due to the enhanced strain localization on friction-stir-welded 5-mm-thick pure copper plates. The hardness of pure copper plate was recorded to be around 65–105 $H_v$ (0.64–1.03 GPa) [10]. In another study, micro-alloyed copper and pure copper powders were prepared in powder form by inert gas atomization with a mean particle size of 30 µm. Tensile, microhardness tests, and instrumented indentation were employed to determine the mechanical properties of those powders. The corresponding data at maximum indentation depth were obtained as $2.2 \pm 0.5$ and $136.5 \pm 12.4$ GPa for hardness and Young's modulus, respectively [11]. Kucharski et al. measured the hardness values for single crystalline copper specimens with different orientations [(001), (011) and (111)] using Oliver–Pharr method. The values of hardness and Young's modulus without holding at peak indentation force were reported as 0.775, and 110 GPa, respectively. On the other hand, for 60 s holding time, the hardness was 0.536 GPa, while Young's modulus was reported as 72 GPa [12].

The present work aimed for investigating the mechanical properties of spherical copper powders (−25 to −110 micron size range) which were compacted onto copper substrate, first, and then subjected to sintering. Such features are referred as to surface modulation and/or surface texturing. Manufacturing of such surface modulations and their heat transfer efficiencies were studied by a group of researchers including the last author of current manuscript, earlier [4, 5, 13]. The current research interest is to determine the effect of manufacturing and post-process conditions on the mechanical properties of compacted copper powders. To this goal, indentations were performed on the powders at different features of compact and hardness values were compared. In addition, finite element model of indentation was established and it was verified with the indentation force–displacement data obtained from indentation.

## 2 Experimental details

### 2.1 Background on instrumented indentation

In indentation measurement, an indenter, usually pyramidal in shape, is used to make imprint on the surface of interest. Forces involved during indentation are usually in milli- or micro-Newton range, and force–displacement depth is continuously recorded and independently controlled. The force–displacement curves are generated automatically. The reduced elastic modulus $E_r$ and sample hardness $H$ are calculated according to the ISO-14577 standard [14].

The hardness is defined as the ratio of the peak indentation test force, $F_{max}$, to the projected area of the indentation impression, $A_c$. For a perfect Berkovich indenter, the projected contact area, $A_c$, is a function of the contact depth, $h_c$, and it is expressed as follows [15]:

$$A_c = \pi.\tan^2\emptyset\, h_c^2 = 24.56\, h_c^2 \tag{1}$$

where $\emptyset = 70.32°$ and represents the effective semi-angle of the conical indenter equivalent to the Berkovich one. The contact depth, $h_c$, is determined using depth-sensing indentation technique. In this method, first, the force–displacement depth of unloading section is fit to a simple power-law equation:

$$P = \alpha\left(h - h_f\right)^m \tag{2}$$

where α, $h_f$ and m are fitting parameters. The contact stiffness at peak load is calculated from these parameters $\left(S = dP/dh|P_{max}\right)$. Then, the contact depth $h_c$ is calculated using $S$, $h_{max}$ and $P_{max}$ as follows:

$$h_c = h_{max} - \varepsilon\frac{P_{max}}{S} \tag{3}$$

where $\varepsilon = 0.72$ for a conical tip. The hardness is thus calculated as follows:

$$H = \frac{F_{max}}{A_c} = \frac{F_{max}}{24.56h_c^2} \tag{4}$$

Maximum indentation force–displacement behavior can also effectively be used in determining the reduced modulus of elasticity, $E_r$, as given in either of the below equations:

$$E_r = \frac{\sqrt{\pi}}{2}\frac{S}{\sqrt{A_c}} \tag{5}$$

or

$$\frac{1}{E_r} = \frac{1-\nu_s^2}{E_s} + \frac{1-\nu_i^2}{E_i} \tag{6}$$

where $E_s$ and $E_i$ are the modulus of elasticity of specimen and indenter, respectively. $\nu_s$ and $\nu_i$ are Poisson's ratio of the specimen and indenter tip, respectively. $E_r$, on the other hand, is the reduced elasticity modulus of the material and can be calculated from the unloading part of the continuous force–displacement curve. Material properties for the Berkovich indenter used in this study are $\nu_i = 0.07$ and $E_i = 1140$ GPa.

### 2.2 Sample preparation and indentation

The sample of interest was chosen as Cu powders that were compacted in a die with channels to yield a porous surface modulation in conical shape on a copper substrate. 100 dimples were obtained on a copper sheet 55 mm in diameter and 0.2 mm in thickness as it is shown in Fig. 1a. The samples, were then subjected to sintering at controlled atmosphere for 1 h. As it is shown in Fig. 1b, c, each dimple has 1 mm base diameter and 500 μm height. Powders in different size ranges were utilized to obtain controlled porosity. For example, powders with relatively smaller size (e.g. 0–25, 25–45, 43–65 μm) were used for valley and lower feature while upper feature consisted of powders in 90–106 μm range as it can be noticed from Fig. 1c. The details of specimen manufacturing can be found elsewhere in the literature [13].

In indentation tests, UMT-2 Nano + Micro Tribometer (Bruker Inc., Billerica, MA, USA) was used. The porous surface structures were first prepared in regular microscopic examination sample form, and then indentations were performed on individual powders at lower feature, upper feature, and Cu substrate sheet. The maximum indentation force of 50 mN was determined upon trials by employing different peak loads and ensuring the repeatability of results. All the measurements were performed at room temperature. It should be noted that indentations with smaller peak loads may result in insufficient deformation (just distorted crystal lattice), and/or local grain boundary response [17, 18]. Therefore, sufficiently high peak loads should be employed to create geometrically necessary dislocations, and hence representative microstructural behavior. The selected peak load was found be in agreement with the ones reported in relevant literature, as well [17–21].

Apart from the modulus of elasticity and hardness measurements through indentation tests, statistical analyses were also performed to reveal the significance of the variation on hardness and modulus of elasticity data. One-way ANOVA tests with $p < 0.05$ were applied to determine important differences between modulus of elasticity and hardness.

### 2.3 Finite element modeling of indentation

To reveal the evolution of stress and strain values during the indentation, the process was modeled by means of a commercially available FEA software package MSC Marc (MSC Software Corp., Santa Ana, CA, USA). Only the indentation

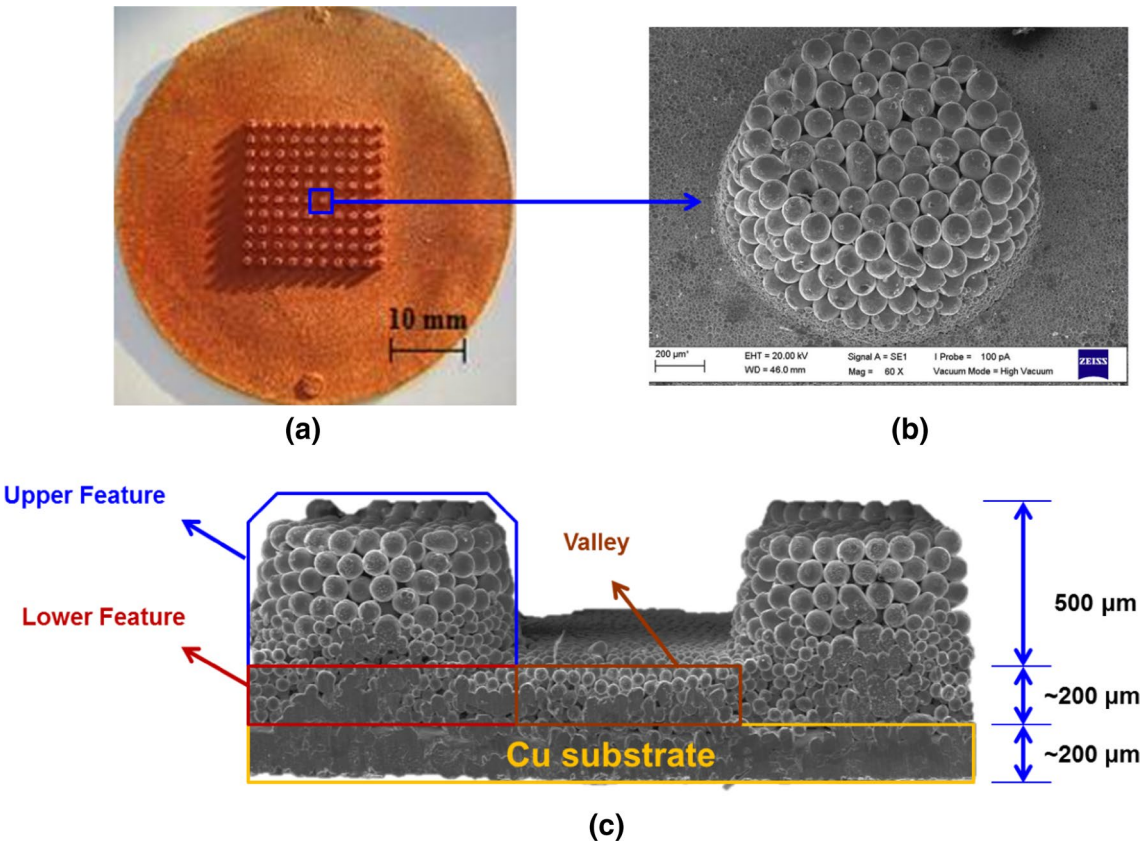


**Fig. 1** **a** Photo of compacted and sintered copper powders onto the surface; **b** SEM micrograph of compacted powders (top view); **c** SEM micrograph of compacted powders and descriptions for different features in the compact (front view)

on Cu substrate part of specimen was modeled for simplicity. To this goal, the force–displacement data obtained from indentation measurements was used as input in FEA, and stress–strain variation during the indentation process was acquired.

It was shown by Lichinchi et al. that the difference between the 3-D modeling with pyramid-shaped Berkovich indenter and 2-D modeling with corresponding conical indenter is negligible. Therefore, 2-D axisymmetric model of indentation was established that reduced the computational time. The Berkovich indenter used in indentation can be converted to the conical shape with half-apex angle of 70.3° [22]. The Berkovich pyramid is replaced with an equivalent cone possessing the same projected area vs. indentation depth $h$ to describe analytically the indenter tip nanodeviations from the ideal sharp tip geometry (Fig. 2) [23]. The angle $\theta$ of the equivalent cone can be calculated according to the following equations:

$$r_{eq} = \frac{1}{2}(a)\sqrt{\frac{\tan 60^\circ}{\pi}} \tag{7}$$

$$\tan\theta = \frac{r_{eq}}{h} \tag{8}$$

where $a$ is the pyramidal base side length measured in mm, $r_{eq}$ is the radius of the equivalent indenter conical area and $h$ is the cone height.

Figure 3 shows the axisymmetric model of corresponding conical rigid indenter and the specimen along with the boundary conditions applied. The displacement of the specimen is restricted along the $x$- and $y$-axes (vertical, and horizontal), and centerline. The specimen, different from the real case, was considered as a homogeneous solid and modeled with 1950 four-node axisymmetric quadrilateral, full integration elements. Fine mesh was preferred for the specimen around the contact area. The Poisson's ratio and the modulus of elasticity of the pure copper material was taken as 0.343 and 110 GPa in the finite elements simulation [24]. The yield and tensile strength of annealed pure copper on the other hand was taken as 255 and 620 MPa, respectively [25]. The coefficient of friction between the indenter and the specimen was set to zero, which was reported as a minor factor in the literature [26].

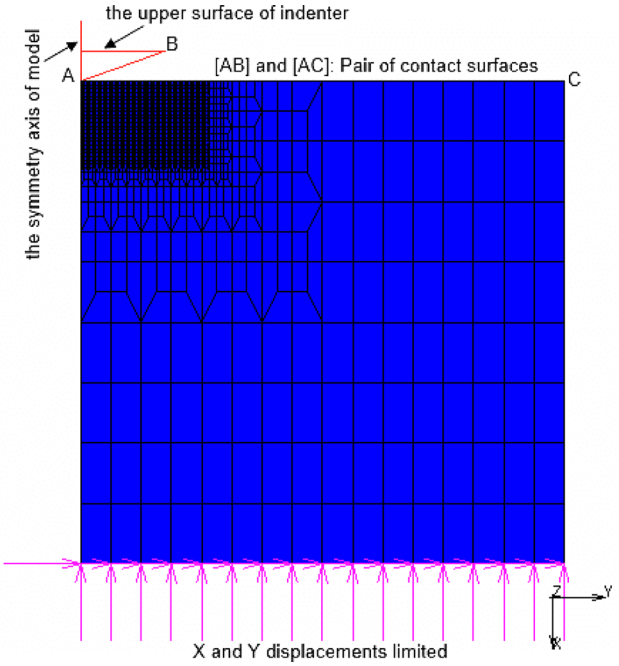


**Fig. 3** Boundary conditions applied on the 2-D axisymmetric finite element model

Both loading and unloading steps of indentation process were simulated through FEA. The displacement data of force–displacement curve of the copper substrate obtained at force level 50 mN were used as input for the movement of indenter in FE model. The force–displacement data obtained from FE analyses with different number elements were compared with the experimental data to optimize the number of

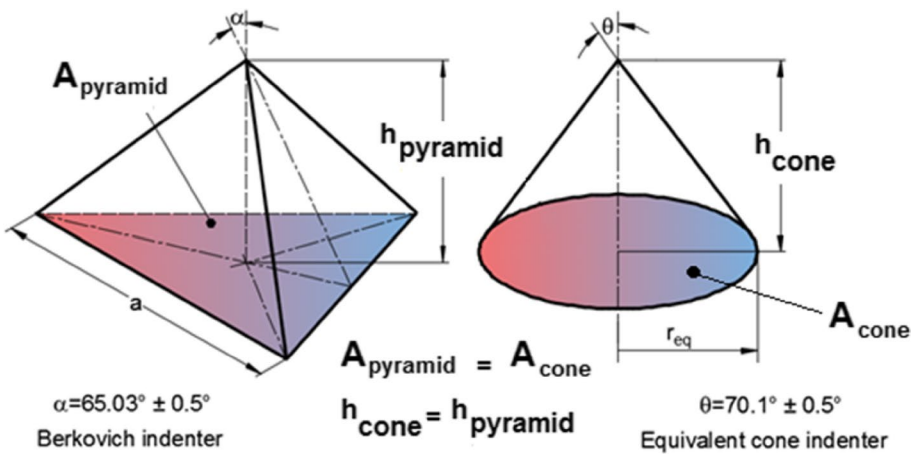


**Fig. 2** Replacement of a Berkovich pyramid indenter with an equivalent cone [23]

elements to be used in modeling. Therefore, different trials were performed as it is seen in Fig. 4. It was found that when the workpiece is modeled with ~2000 elements, force–displacement curve obtained from FEA satisfactorily converges to the one obtained from indentation as it is seen in Fig. 4. This number of elements was also found to be appropriate as the indentation force value converges to 50 mN preset value when more than 1000 elements are used to model the workpiece (Fig. 5).

## 3 Results and discussion

### 3.1 Force–displacement curves

At least nine measurements were taken to report a hardness and modulus of elasticity value. Figure 6 shows a typical force–displacement plot obtained with 50 mN maximum indentation force at upper feature powder compacts. The curve indicates that the pure copper specimen exhibited elastoplastic deformation behavior during the indentation. The applied peak force was 50 mN with a loading rate of 0.1 mN/s. Similar indentation force–displacement curves were obtained at different features of compact.

### 3.2 Microindentation results

The modulus of elasticity obtained from different features of Cu compact are compared in Fig. 7a. The modulus of elasticity values for both lower and upper features of compacted powders were recorded as 70 GPa. The average modulus of elasticity for copper substrate sheet is 100 GPa. Relatively higher variations were observed for the values obtained for powders. The scattered data for modulus of elasticity values obtained from powders are attributed to the non-uniform plastic deformation of pure Cu during compaction. The one-way ANOVA was performed to reveal the possible differences among modulus of elasticity values. It was found that

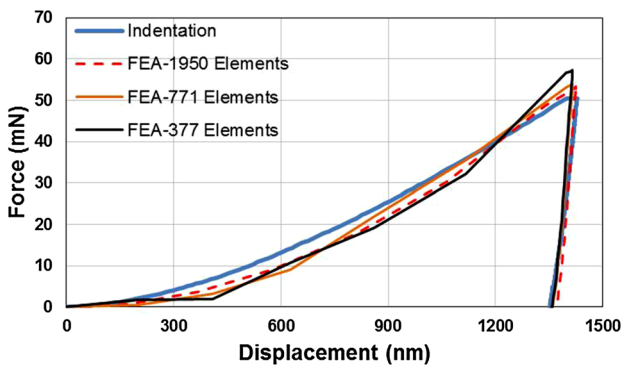


**Fig. 4** Comparison on the force–displacement curves from indentation test and simulations with different number of elements

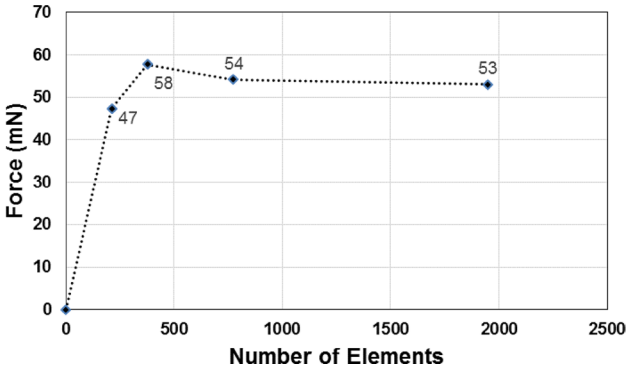


**Fig. 5** Variation of indentation force with the number of elements used in the 2-D axisymmetric finite element model

the changes in modulus of elasticity values are insignificant. Depending on the measurement location (substrate or features), the modulus of elasticity values were recorded as in the range of 70–114 GPa for substrate and Cu powders at lower and upper features of the compaction.

The hardness values obtained from compacted sample are given in Fig. 7b. Each hardness and modulus of elasticity

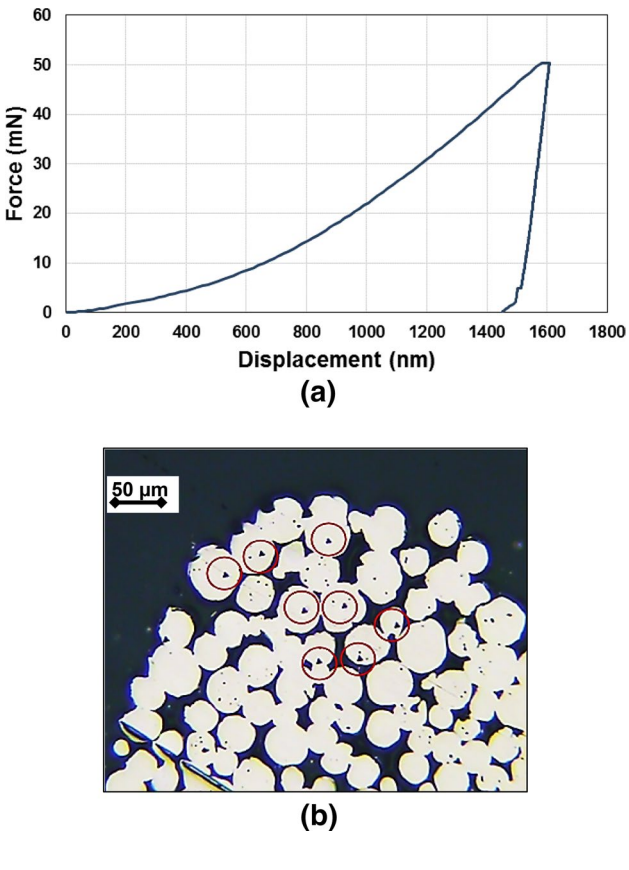


**Fig. 6** **a** Force–displacement curve obtained from sintered copper powder at upper feature and **b** optical microscope image of indentation area

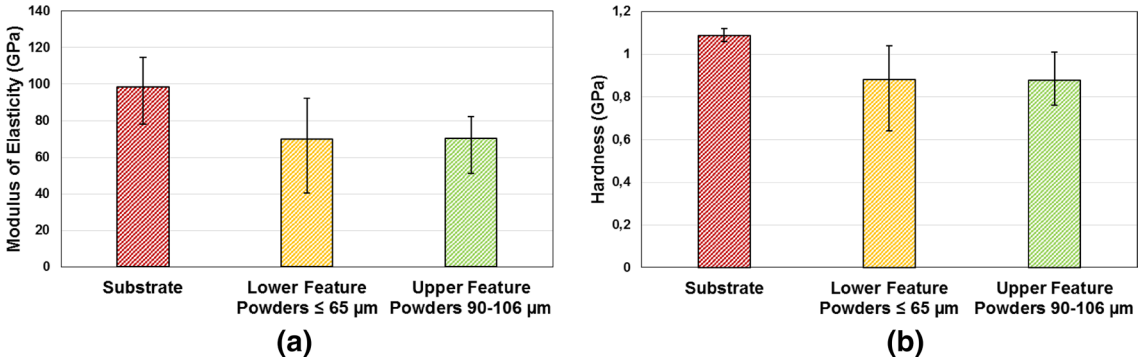


**Fig. 7** **a** Modulus of elasticity and **b** hardness values obtained with 50 mN peak indentation force for Cu substrate, lower and upper features

value were reported as average of at least nine indentation performed under same conditions. The hardness values were recorded in the range of 0.87–1.12 GPa for Cu sheet (substrate) and powders (lower and upper features of the compaction). Considerably small differences in the hardness values were observed between lower feature and upper feature (0.88 vs. 0.87 GPa) of compacts. Average hardness value for substrate, on the other hand, was measured as 1.06 GPa. The one-way ANOVA was performed to reveal the possible differences among hardness values. Similar to the modulus of elasticity values, it was found that the changes in hardness values are insignificant.

In macroscale, the hardness (in MPa) is roughly equal to three times of yield strength value for metals. That simple linear relation can be given with the following equation:

$$H = c \times S \tag{9}$$

where $H$ is hardness, $S$ is uniaxial flow strength of the material, and $c$ is referred as the elastic constraint factor [27]. It was noted that $c$ value changes in the range of 2.50–4.28 considering the lower, upper and substrate values of yield strength as 255 MPa [25].

### 3.3 Pile-up analysis

The work-hardening characteristics of a material dictate the deformation behavior underneath the indenter tip. Pile-up and sink-in are two common phenomena in nanoindentation that significantly either underestimate or overestimate the contact area, consequently the results. In pile-up, the material around the contact area tends to deform in the upward direction, whereas in sink-in it deforms in downward direction [28, 29]. In pile-up, the contact area is underestimated and as a consequence, modulus of elasticity and hardness values are overestimated. This issue is more pronounced when dealing with soft coatings on hard substrates. In sink-in, on the other hand, the contact area is overestimated and, therefore, modulus of elasticity and hardness values are underestimated [6]. Pile-up is more encountered for well-annealed soft metal or material with low strain-hardening potential while sink-in is more pronounced for strain-hardened materials and metallic glasses with low strain-hardening rate [7, 28, 29]. It was also reported by Moharrami and Bull that effect of pile-up increases with increasing indentation force and it can deviate from the real values as high as 15% for the Young's modulus and 35% for the hardness values [6]. The most common way to investigate whether the pile-up or sink-in occurred is to check the $h_f/h_{max}$ ratio, where $h_f$ is final indentation depth and $h_{max}$ is the maximum indentation depth recorded. This ratio can take values between 0 and 1. The lower limit (0) denotes the fully elastic case while the upper limit value (1) corresponds to rigid-plastic behavior. This ratio can easily be obtained from the unloading curve of nanoindentation. It was noted by Oliver and Pharr that when $h_f/h_{max}$ ratio is greater than 0.7, pile-up effect is likely to be experienced [30]. Figure 8 illustrates the $h_f/h_{max}$ values obtained for substrate, lower and upper features. As it can be seen from the figure the ratio was obtained in the range of 0.90–0.97 (far greater than 0.7) and one can expect pile-up effects. Nonetheless, since the copper powders were subjected to sintering after compaction those got the work-hardening property and pile-up

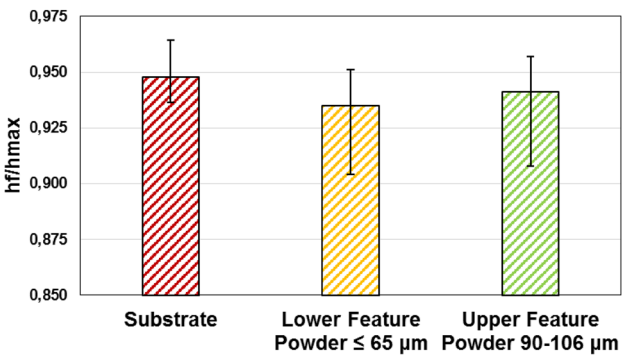


**Fig. 8** $h_f/h_{max}$ values for pure Cu substrate, lower and upper features

was not experienced. Similar results were reported by Gale and Achuthan as they noted that $h_f/h_{max}$ ratio may not be accurately used in quantitatively correlating pile-up characteristics [31].

### 3.4 FEA of indentation

Figure 9 shows the variation of equivalent von Mises stress for the copper substrate after the indenter tip reached the maximum penetration depth. During the loading stage, the indenter was driven into the specimen surface in the axial direction for a specific depth in 100 s and with a constant speed. This provides the loading part of the force–displacement curve in the finite element simulation. When the indenter tip reached the preset maximum penetration depth (~ 1400 nm) the test specimen was unloaded, and the indenter tip returned to its initial position with the same speed as that of the loading stage. Hence, the unloading part of the force–displacement curve is obtained from FEA. The highest value of equivalent von Mises stress was noted as around 900 MPa around the tip of indenter.

Figure 10 shows a typical force–displacement curve obtained from indentation and finite element simulation result obtained with 50 mN force for substrate. It can be seen from the figure that the force–displacement curves obtained from finite element analysis was quite well in agreement with the experimental data especially in unloading part of indentation.

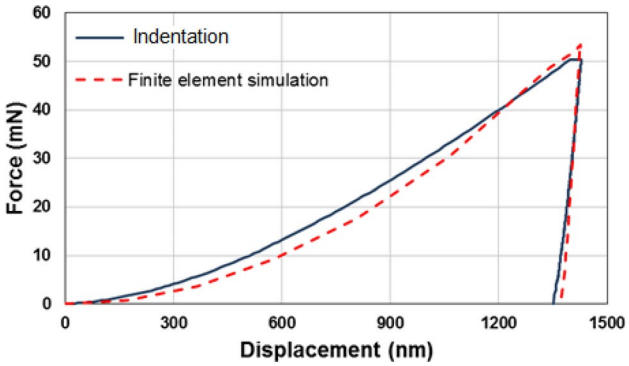


**Fig. 10** Force–displacement curve and simulation results for substrate feature of pure copper

## 4 Conclusion

This study aimed to determine mechanical properties compacted and sintered spherical copper powders. Microindentations were performed at three different regions, namely substrate, upper and lower features of the compact. The following are the main outcomes of this research:

- Microindentations on the copper substrate were performed with 50 mN indentation peak load; and modulus of elasticity values were recorded in the range of 78–111 GPa, while hardness values were in the range of 1.06–1.12 GPa.
- Indentations with the same peak loading on lower and upper features of the compact yielded average hardness and modulus of elasticity values as 0.88, and 70.1 GPa, respectively. In all instances, the modulus of elasticity

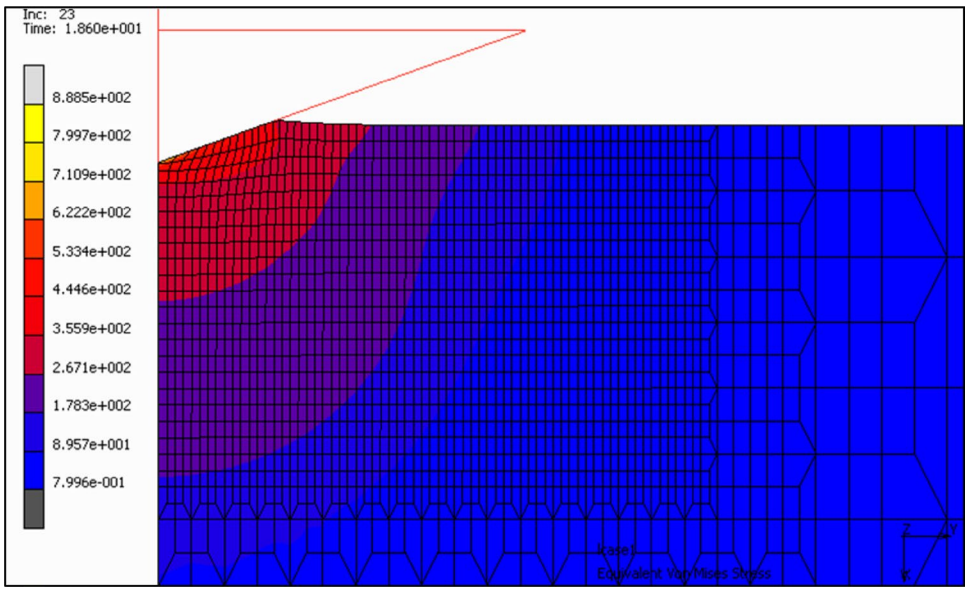


**Fig. 9** Variation of equivalent von Mises stress for pure copper after the indenter tip reached the maximum penetration depth

of the material increased with increasing hardness. In addition, the modulus of elasticity of the Cu substrate was found to be slightly higher than those for lower and upper features.

- One-way ANOVA analyses (for $p \leq 0.05$) were performed to check the possible differences in results, yet it was revealed that changes in both modulus of elasticity and hardness values with peak indentation force are insignificant for the force level (50 mN) experimented.
- FE model of indentation was established and displacement of the indenter was used as input in FE analyses. It was found that the force–displacement curves obtained from the finite element simulation were in very good agreement with actual data obtained from the indentation.

**Acknowledgements** The authors are grateful to Gaziosmanpaşa University for sharing their lab capabilities and their assistance in indentation measurements. The help of BİAS Engineering's personnel in FE modeling-related issues is also acknowledged.

**Compliance with ethical standards**

**Conflict of interest** The authors declare that they have no conflict of interest.

## References

1. T. Falat, P. Matkowski, B. Płatek, C. Zandén, J. Felba, L.L. Ye, J. Liu, Investigation on interaction between indium based thermal interface material and copper and silicon substrates, in *Microelectronics Packaging Conference* (Grenoble, 2013), pp. 1–5
2. R.M. German, *Sintering Theory and Practice* (Wiley, Hoboken, 1996), p. 555
3. Copper Development Association Inc. https://www.copper.org/education/c-facts/electronics/print-category.html. Accessed 17 Nov 2016
4. O.N. Cora, D. Min, M. Koç, M. Kaviany, Microscale-modulated porous coatings: fabrication and pool-boiling heat transfer performance. J. Micromech. Microeng **20**(3), 035020 (2010)
5. D.H. Min, G.S. Hwang, Y. Usta, O.N. Cora, M. Koc, M. Kaviany, 2-D and 3-D modulated porous coatings for enhanced pool boiling. Int. J. Heat. Mass. Trans **52**(11–12), 2607–2613 (2009)
6. S.J. Bull, N.A. Moharrami, A comparison of nanoindentation pile-up in bulk materials and thin films. Thin Solid Films **572**, 189–199 (2014)
7. K.W. McElhaney, J.J. Vlassak, W.D. Nix, Determination of indenter tip geometry and indentation contact area for depth-sensing indentation experiments. J. Mater. Res. **13**(5), 1300–1306 (1998)
8. K.R. Narayanan, S. Subbiah, I. Sridhar, Indentation response of single-crystal copper using rate-independent crystal plasticity. Appl. Phys. A **105**(2), 453–461 (2011)
9. T.H. Wang, T.H. Fang, Y.C. Lin, Finite-element analysis of the mechanical behavior of Au/Cu and Cu/Au multilayers on silicon substrate under nanoindentation. Appl. Phys. A **90**(3), 457–463 (2008)
10. P. Xue, G.M. Xie, B.L. Xiao, Z.Y. Ma, L. Geng, Effect of heat input conditions on microstructure and mechanical properties of friction-stir-welded pure copper. Metall. Mater. Trans. A **41**(8), 2010–2021 (2010)
11. N. Kang, P. Coddet, H. Liao, C. Coddet, Cold gas dynamic spraying of a novel micro-alloyed copper: microstructure, mechanical properties. J. Alloy. Compd **686**, 399–456 (2016)
12. S. Kucharski, D. Jarząbek, A. Piątkowska, S. Woźniacka, Decrease of nano-hardness at ultra-low indentation depths in copper single crystal. Exp. Mech **56**(3), 381–393 (2016)
13. B. Öztürk, Ö.N. Cora, M. Koç, Effect of sintering temperature on the porosity and microhardness of the micro-scale 3-D porous gradient surfaces, in *8th International Conference Multi-Material Micro Manufacture*, (2011), pp. 176–179
14. International Organization for Standardization, *ISO 14577-1 Metallic materials, Part 1: Test method*. (International Organization for Standardization, Geneva, 2015)
15. A.C. Fischer-Cripps, Critical review of analysis and interpretation of nanoindentation test data. Surf. Coat. Tech **200**(14–15), 4153–4165 (2006)
16. F.M. Borodich, The Hertz-type and adhesive contact problems for depth-sensing indentation. Adv. Appl. Mech **47**, 225–366 (2014)
17. S. Bigl, T. Schöberl, S. Wurster, M.J. Cordill, D. Kiener, Correlative microstructure and topography informed nanoindentation of copper films. Surf. Coat. Technol. **307**, 404–413 (2016)
18. S. Vincent, B.S. Murty, M.J. Kramer, J. Bhatt, Micro and nano indentation studies on $Zr_{60}Cu_{10}Al_{15}Ni_{15}$ bulk metallic glass. Mater. Des. **65**, 98–103 (2015)
19. B. Bose, R.J. Klassen, Effect of copper addition and heat treatment on the depth dependence of the nanoindentation creep of aluminum at 300 K. Mater. Sci. Eng. A **500**, 164–169 (2009)
20. D. Galusek, F.L. Riley, The influence of sintering additives on the indentation response of liquid-phase-sintered polycrystalline aluminas. Philos. Mag. A **82**, 2041–2057 (2002)
21. W. Li, C. Huang, M. Yu, H. Liao, Investigation on mechanical property of annealed copper particles and cold sprayed copper coating by a micro-indentation testing. Mater. Des. **46**, 219–226 (2013)
22. M. Lichinchi, C. Lenardi, J. Haupt, R. Vitali, Simulation of Berkovich nanoindentation experiments on thin films using finite element method. Thin Solid Films **312**(1–2), 240–248 (1998)
23. K.D. Bouzakis, M. Pappa, G. Maliaris, N. Michailidis, Fast determination of parameters describing manufacturing imperfections and operation wear of nanoindenter tips. Surf. Coat. Tech **215**, 218–223 (2013)
24. J. Appa Rao, J. Babu Rao, S. Kamaluddin, M.M.M. Sarcar, N.R.M.R. Bhargava, Studies on cold workability limits of pure copper using machine vision system and its finite element analysis. Mater. Design **30**(6), 2143–2151 (2009)
25. S. Kalpakjian, S.R. Schmid, H. Musa, Mechanical behavior, testing, and manufacturing properties of materials. 6th edn. Manuf. Process. Eng. Mater. Pearson Education, USA, pp. 80–84 (2009)
26. X. Chen, N. Ogasawara, M. Zhao, N. Chiba, On the uniqueness of measuring elastoplastic properties from indentation: the indistinguishable mystical materials. J. Mech. Phys. Solids **55**(8), 1618–1660 (2007)
27. E.J. Pavlina, C.J. Van Tyne, Correlation of yield strength and tensile strength with hardness for steels. J. Mater. Eng. Perform **17**(6), 888–893 (2008)
28. C.A. Charitidis, E.P. Koumoulos, V. Nikolakis, D.A. Dragatogiannis, Structural and nanomechanical properties of a zeolite

membrane measured using nanoindentation. Thin Solid Films **526**, 168–175 (2012)
29. S. Kucharski, D. Jarzabek, Depth dependence of nanoindentation pile-up patterns in copper single crystals. Metall. Mater. Trans. A **45**(11), 4997–5008 (2014)
30. W.C. Oliver, G.M. Pharr, Measurement of hardness and elastic modulus by instrumented indentation: advances in understanding and refinements to methodology. J. Mater. Res. **19**(1), 3–20 (2004)
31. J.D. Gale, A. Achuthan, The effect of work-hardening and pile-up on nanoindentation measurements. J. Mater. Sci **49**(14), 5066–5075 (2014)